

# Gene therapy rescues cilia defects and restores olfactory function in a mammalian ciliopathy model

Jeremy C McIntyre<sup>1</sup>, Erica E Davis<sup>2-4</sup>, Ariell Joiner<sup>1</sup>, Corey L Williams<sup>1</sup>, I-Chun Tsai<sup>2,4</sup>, Paul M Jenkins<sup>1</sup>, Dyke P McEwen<sup>1</sup>, Lian Zhang<sup>1</sup>, John Escobado<sup>1</sup>, Sophie Thomas<sup>5</sup>, Katarzyna Szymanska<sup>6</sup>, Colin A Johnson<sup>6</sup>, Philip L Beales<sup>7</sup>, Eric D Green<sup>8</sup>, James C Mullikin<sup>8</sup>, NISC Comparative Sequencing Program<sup>8</sup>, Aniko Sabo<sup>9</sup>, Donna M Muzny<sup>9</sup>, Richard A Gibbs<sup>9</sup>, Tania Attié-Bitach<sup>5</sup>, Bradley K Yoder<sup>10</sup>, Randall R Reed<sup>11</sup>, Nicholas Katsanis<sup>2-4</sup> & Jeffrey R Martens<sup>1</sup>

**Cilia are evolutionarily conserved microtubule-based organelles that are crucial for diverse biological functions, including motility, cell signaling and sensory perception<sup>1</sup>. In humans, alterations in the formation and function of cilia manifest clinically as ciliopathies, a growing class of pleiotropic genetic disorders<sup>2-4</sup>. Despite the substantial progress that has been made in identifying genes that cause ciliopathies, therapies for these disorders are not yet available to patients. Although mice with a hypomorphic mutation in the intraflagellar transport protein IFT88 (*Ift88*<sup>Tg737Rpw</sup> mice, also known as ORPK mice)<sup>5</sup> have been well studied, the relevance of IFT88 mutations to human pathology is unknown. We show that a mutation in *IFT88* causes a hitherto unknown human ciliopathy. *In vivo* complementation assays in zebrafish and mIMCD3 cells show the pathogenicity of this newly discovered allele. We further show that ORPK mice are functionally anosmic as a result of the loss of cilia on their olfactory sensory neurons (OSNs). Notably, adenoviral-mediated expression of IFT88 in mature, fully differentiated OSNs of ORPK mice is sufficient to restore ciliary structures and rescue olfactory function. These studies are the first to use *in vivo* therapeutic treatment to reestablish cilia in a mammalian ciliopathy. More broadly, our studies indicate that gene therapy is a viable option for cellular and functional rescue of the complex ciliary organelle in established differentiated cells.**

The increasing number of ciliopathy disorders accentuates the importance of cilia and their function in mammalian cells<sup>1-3</sup>. These diseases, including Bardet-Biedl syndrome, Meckel-Gruber syndrome (MKS), nephronophthisis, Joubert syndrome and Jeune asphyxiating thoracic dystrophy (JATD), are heterogeneous disorders caused by mutations

in genes encoding proteins that are required for the structural integrity, functional integrity or both of the primary cilium<sup>5</sup>. In addition to renal cysts, polydactyly, *situs inversus*, obesity and cognitive and sensory defects accompany many of these disorders. These defects include blindness, neurosensory hearing loss, altered nociception and anosmia<sup>5-7</sup>. Loss of olfactory function orthologous to that found in the human pathology has been identified in rodent models with mutations or deletions in Bardet-Biedl Syndrome and nephronophthisis genes, suggesting that olfactory deficits are probably pathognomonic of multiple ciliopathies<sup>6-8</sup>.

Ciliopathy phenotypes encompass an array of defects in cilia signaling, assembly and maintenance<sup>9-13</sup>. An essential part of building and maintaining cilia is the process of intraflagellar transport (IFT)<sup>1,14,15</sup>. Loss-of-function mutations in several IFT genes have been found in patients with a ciliopathy, indicating that IFT proteins are potentially important clinical targets<sup>16-19</sup>. However, in most mouse models, IFT-null alleles are embryonic lethal, making it challenging to develop a vertebrate model that can be tested for potential therapeutic treatments<sup>20-23</sup>.

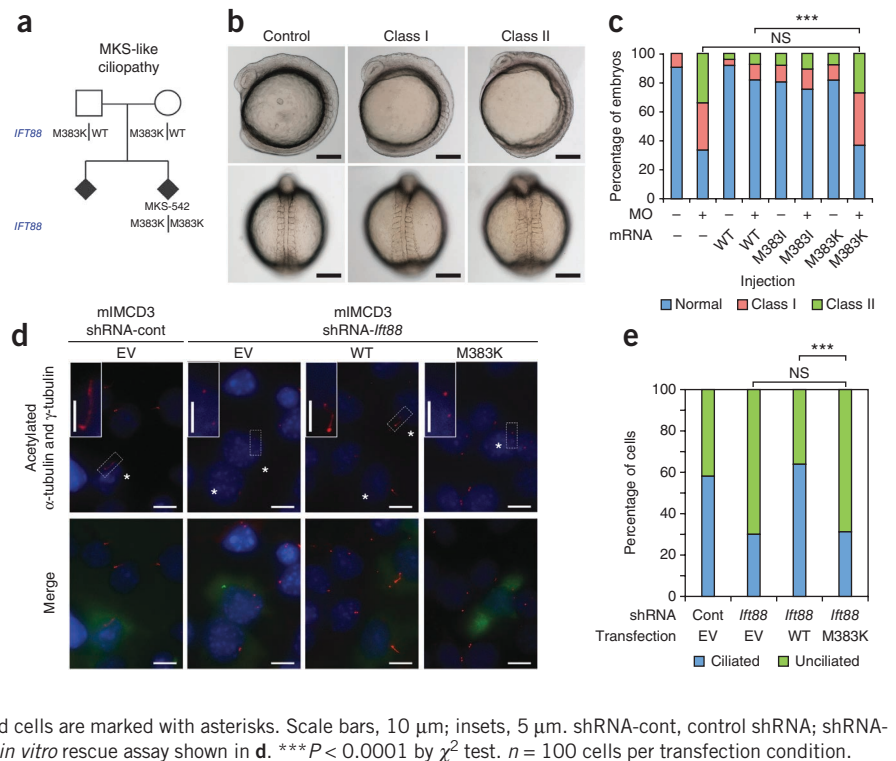
One notable exception is the mouse model of Oak Ridge Polycystic Kidney disease (the ORPK mouse), in which cilia dysfunction arises from a hypomorphic mutation in *Ift88* (also known as *Polaris* or *Tg737*)<sup>5</sup>. However, mutations in *IFT88* have not been reported previously in patients with a ciliopathy. To determine the direct relevance of the ORPK mouse model to human genetic disease, we sequenced *IFT88* in a cohort of individuals and fetuses with MKS ( $n = 161$ ) or JATD ( $n = 62$ ), two severe ciliopathies. In one fetus of northern European descent with MKS-like features (MKS-542), we identified a homozygous nonsynonymous change (M383K) that segregated with disease under an autosomal-recessive model (Fig. 1a). This fetus was the second consecutive terminated pregnancy in the pedigree, and

<sup>1</sup>Department of Pharmacology, University of Michigan, Ann Arbor, Michigan, USA. <sup>2</sup>Center for Human Disease Modeling, Duke University Medical Center, Durham, North Carolina, USA. <sup>3</sup>Department of Pediatrics, Duke University Medical Center, Durham, North Carolina, USA. <sup>4</sup>Department of Cell Biology, Duke University Medical Center, Durham, North Carolina, USA. <sup>5</sup>Département de Génétique et INSERM U-781, Hôpital Necker-Enfants Malades, Université Paris Descartes, Paris, France. <sup>6</sup>Section of Ophthalmology and Neurosciences, Leeds Institute of Molecular Medicine, St. James's University Hospital, Leeds, UK. <sup>7</sup>Molecular Medicine Unit, Institute of Child Health, University College London, London, UK. <sup>8</sup>US National Institutes of Health Intramural Sequencing Center, National Human Genome Research Institute, National Institutes of Health, Bethesda, Maryland, USA. <sup>9</sup>Human Genome Sequencing Center, Baylor College of Medicine, Houston, Texas, USA. <sup>10</sup>Department of Cell Biology, University of Alabama at Birmingham, Birmingham, Alabama, USA. <sup>11</sup>Department of Molecular Biology and Genetics, Johns Hopkins University, Baltimore, Maryland, USA. Correspondence should be addressed to J.R.M. (martensj@umich.edu).

Received 4 April; accepted 11 June; published online 2 September 2012; doi:10.1038/nm.2860

**Figure 1** The homozygous M383K mutation in *IFT88* causes an MKS-like ciliopathy.

(a) The *IFT88* M383K variant segregates with disease in an MKS-like pedigree. DNA was unavailable from the affected sibling. (b) Gastrulation defects after suppression of *ift88* in midsomitic zebrafish embryos, including a shortened anterior-posterior axis, small and disorganized anterior structures, kinking and broadening of the notochord and broadened somites. Lateral (top) and dorsal (bottom) views are shown for representative control (unaffected), class I (mild defects) and class II (severe defects) embryos. Scale bars, 250  $\mu$ m. (c) Quantification of embryo batches injected with *ift88* morpholino (MO) and human mRNA showing that M383K is pathogenic according to *in vivo* complementation studies.  $***P < 0.0001$ , NS, not significant by  $\chi^2$  test.  $n = 52$ – $71$  embryos scored per injection with masked scoring, repeated three times. (d) Fluorescent images of representative mIMCD3 cells with enlarged images of cilia from transfected cells (insets) showing that M383K is functionally null. Acetylated  $\alpha$ -tubulin and  $\gamma$ -tubulin (red) indicate cilia and centrosomes; GFP was used as a transfection control (green, bottom row); nuclei are indicated with DAPI staining (blue). EV, empty vector. Transfected cells are marked with asterisks. Scale bars, 10  $\mu$ m; insets, 5  $\mu$ m. shRNA-cont, control shRNA; shRNA-*IFT88*, shRNA targeting *IFT88*. (e) Quantification of the *in vitro* rescue assay shown in d.  $***P < 0.0001$  by  $\chi^2$  test.  $n = 100$  cells per transfection condition.



both of these terminated fetuses showed renal and hepatic cysts without polydactyly or encephalocele. This variant is absent from publicly available genome-wide SNP and sequence databases (dbSNP and 1000 Genomes) and was also absent from 10,750 control chromosomes from individuals of European and African-American descent available through the National Heart, Lung, and Blood Institute Exome Variant Server (ESP, <http://evs.gs.washington.edu/EVS/>) who do not show ciliopathy phenotypes.

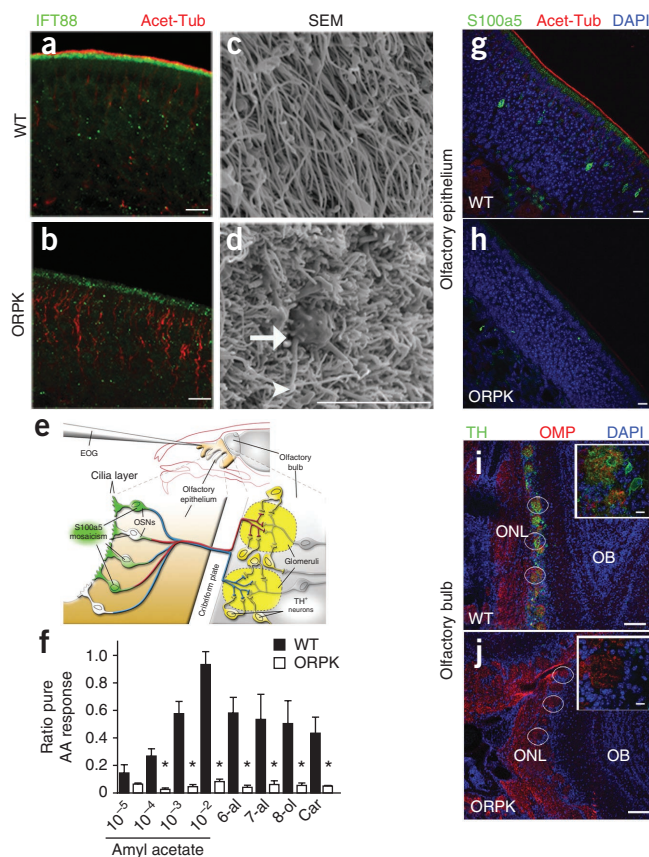
Although our genetic data were suggestive of pathogenicity, we assayed the pathogenic potential of M383K *IFT88* directly by *in vivo* complementation assays in midsomitic zebrafish embryos<sup>18,24–26</sup>. We first suppressed the single *Danio rerio* ortholog of *IFT88* by morpholino (MO) injection and found gastrulation defects that were reminiscent of other IFT gene morphants at the 9–10 somite stage, which included a shortened anterior-posterior axis, disorganized anterior features, a broadened notochord and laterally elongated somites (Fig. 1b,c)<sup>18,24–26</sup>. Co-injection of wild-type (WT) human *IFT88* mRNA with *ift88* MO resulted in a significant rescue of these defects compared to injection of MO alone (18% of embryos were affected after WT *IFT88* injection plus MO compared to 66% affected after MO injection alone;  $P < 0.0001$ ; Fig. 1c). We observed no difference between co-injection of M383K mRNA plus MO and injection of MO alone, suggesting that M383K is a null allele in this assay. Database analyses revealed another common variant at this position, encoding M383I (rs2442455), that probably does not cause disease. The ESP data in dbSNP show that 3.3% (73/2,223) of control individuals without ciliopathy phenotypes are homozygous for the allele encoding M383I. Co-injection of *ift88* MO with M383I *IFT88* mRNA resulted in rescue that was indistinguishable from that resulting from injection of WT *IFT88* mRNA plus MO (Fig. 1c). We corroborated our *in vivo* pathogenicity data *in vitro* using murine inner medullary collecting duct (mIMCD3) cells with an shRNA targeting *IFT88* and ciliary morphometrics as a

physiologically relevant readout (Fig. 1d,e)<sup>18</sup>. Together, these data provide evidence that the M383K *IFT88* variant is functionally null and probably drives disease phenotypes in the MKS-like pedigree.

We also detected the same mutation coding for M383K in the heterozygous state in four additional human MKS or MKS-like samples and two human JATD samples (Supplementary Table 1). Among these six samples, one MKS-like sample harbored a primary mutation in *MKS1* (sample 102; 1448\_1451dupCAGG hom) suggesting that, similar to other IFT genes, defective *IFT88* may act together with other ciliopathy loci to modulate disease severity or specific endophenotypes<sup>18</sup>. Combined allele counts from our cohort compared to those of controls with no ciliopathy phenotypes showed significant enrichment of M383K in the severe ciliopathy samples (1.8% (8/446) of ciliopathy chromosomes compared to 0/10,750 control chromosomes (ESP);  $P < 6.4 \times 10^{-13}$ ).

Taken together, these data indicate that mutations in *IFT88* in humans are not only sufficient to cause disease but are also contributory to the total mutational load in severe ciliopathies. These data also suggest that the ORPK mouse model might be appropriate to develop therapeutic strategies. Gene therapy is an attractive option for treating deficiencies resulting from loss-of-function mutations. Its utility has been shown in sensory tissues such as the retina<sup>27–29</sup>; however, its use has been restricted to correcting defects in signaling proteins. The reversal of defects associated with the loss or malformation of cilia has not been shown and may potentially be a major challenge, as some ciliopathy alleles lead to both structural and functional defects in primary cilia. Given its accessibility to noninvasive nasal delivery, the olfactory system lends itself well to the development of therapeutic modalities. OSNs are maintained even after perturbation of the sensory apparatus and continually self-renew. This plasticity may ameliorate the cell loss and tissue degeneration that often results from cilia dysfunction and allow for more effective treatment.

**Figure 2** Hypomorphic expression of IFT88 leads to olfactory cilia loss and anosmia in ORPK mice. (a,b) Immunostaining showing endogenous IFT88 and acetylated  $\alpha$ -tubulin (Acet-Tub) localization in WT olfactory epithelium and the absence of both in ORPK olfactory epithelium. Scale bars, 10  $\mu$ m. (c,d) Scanning electron microscopy (SEM) images of the surface of the olfactory epithelium. The arrow highlights the dendritic knob, and the arrowhead highlights malformed cilia in the ORPK olfactory epithelium. Scale bar, 5  $\mu$ m. (e) Schematic of the olfactory system showing the locations and methods of activity determination. TH, tyrosine hydroxylase. (f) Quantified data of the EOG responses of WT ( $n = 3$ , filled bars) and ORPK mice ( $n = 4$ , empty bars) to various dilutions of amyl acetate (AA), as well as hexanal (6-al), heptanal (7-al), octanol (8-ol) and carvone (Car). \* $P < 0.05$  by Student's  $t$  test. Data are means  $\pm$  s.e.m. (g,h) Immunostaining showing mosaic S100a5 expression in WT olfactory epithelium and its loss in ORPK olfactory epithelium. Scale bars, 10  $\mu$ m. (i,j) Immunostaining showing the presence of tyrosine hydroxylase (TH) and olfactory marker protein (OMP) in WT olfactory bulb and the absence of tyrosine hydroxylase staining in ORPK olfactory bulb. Individual glomeruli within the olfactory bulbs are circled. Insets show a single glomerulus. OB, olfactory bulb; ONL, olfactory nerve layer. Scale bars, 50  $\mu$ m; insets, 10  $\mu$ m.



Therefore, we used the ORPK mouse to study the consequences of reduced abundance of IFT88 on olfactory function and investigate whether we can achieve therapeutic rescue of the cellular and functional ciliopathy phenotypes in mammals.

OSNs extend a single dendrite that terminates into a knob from which numerous cilia project. In WT mice, endogenous IFT88 localizes to the apical surface of the olfactory epithelium and is colocalized with acetylated  $\alpha$ -tubulin, the canonical marker for cilia (Fig. 2a). The amounts of both endogenous IFT88 and acetylated  $\alpha$ -tubulin in the olfactory epithelium of ORPK mice are markedly reduced, indicating a loss of olfactory cilia (Fig. 2b). Scanning electron microscopy confirmed this loss, as the surfaces of the olfactory turbinates in ORPK mice showed diminished cilia (Fig. 2c,d) and exposure of the underlying sustentacular cell microvilli. The remaining cilia in ORPK mice were shortened and malformed (Fig. 2d). In agreement with the loss of cilia, the apical localization of the olfactory signaling proteins adenylyl cyclase type III (ACIII), cyclic nucleotide gated channel  $\alpha$  2 (CNGA2) and Gyl3 were also lost in ORPK mice, although the overall thickness of the olfactory epithelium was unaltered (Supplementary Fig. 1a–d). These data show that normal expression of IFT88 is necessary for the maintenance of olfactory cilia.

Given their loss of olfactory cilia, we hypothesized that olfactory function in ORPK mice is severely compromised. We measured olfactory function in these mice by testing changes in odorant-evoked activity in populations of OSNs and individual OSNs, as well as at the synaptic network level (Fig. 2e). Electro-olfactogram (EOG) recordings provide a measure of the summated generator potential from populations of OSNs in response to acute olfactory stimulation. As hypothesized, ORPK mice had markedly reduced responses to all the odorants tested compared to WT littermates (Fig. 2f and Supplementary Fig. 1e). We then analyzed the expression pattern in OSNs of S100a5, a calcium binding protein whose expression correlates with odorant-induced neuronal activity<sup>30</sup>. The WT olfactory epithelium showed a mosaic pattern of S100a5 expression across the OSNs (Fig. 2g), whereas S100a5 expression was virtually absent in ORPK mice (Fig. 2h). In addition, the odor-evoked synaptic activity of OSNs modulates tyrosine hydroxylase expression in a subpopulation of dopaminergic juxtglomerular interneurons<sup>31</sup> within the olfactory glomeruli (Fig. 2e). In WT mice, intense tyrosine hydroxylase staining was associated with all glomeruli, as indicated by the coalescence

of olfactory marker protein (OMP)<sup>+</sup> axons (Fig. 2i). In contrast, in the olfactory bulbs of ORPK mice, tyrosine hydroxylase staining was nearly absent (Fig. 2j and Supplementary Fig. 1f). Co-staining of ORPK olfactory bulb sections for OMP showed the OSN axons coalescing to form glomeruli (Fig. 2j), indicating that the reduced synaptic activity of the OSNs was not a consequence of loss of glomerulus formation. Together, these data show that ORPK mice are functionally anosmic and that OSNs lacking olfactory cilia are unable to propagate odor-stimulated synaptic activity to the olfactory bulb.

For patients suffering from pleiotropic ciliopathies, the ability to restore cilia structures to differentiated cells offers the possibility of correcting these functional defects. As OSNs are amenable to infection by adenovirus<sup>32,33</sup>, we hypothesized that adenovirus-mediated expression of IFT88 in the OSNs would be able to correct the olfactory defects in ORPK mice. To rescue the ORPK anosmia phenotype, we generated an IFT88–GFP fusion protein for expression in OSNs by adenoviral infection. We first examined WT mice by intranasally injecting them with IFT88–GFP adenovirus on postnatal days 7, 8 and 9 (P7, P8 and P9) and analyzing expression of the virus 10 days later. IFT88–GFP localized specifically to the apical surface (Supplementary Fig. 2a–c) of the olfactory epithelium but was not present in OSN axons, identical to the localization of endogenous IFT88 (Supplementary Fig. 2d–i). En face images of IFT88–GFP (Supplementary Fig. 2j) and immunostaining for endogenous IFT88 (Supplementary Fig. 2k) showed enrichment of both in the proximal regions of cilia and localization of IFT88–GFP was indistinguishable between the fixed and the live olfactory tissue (Supplementary Fig. 2l). Co-infection of WT OSNs with IFT88–GFP and a second cilia marker, Arl13b–mCherry, which marks the full length of olfactory cilia, revealed GFP puncta, that are likely IFT trains<sup>15</sup>, along

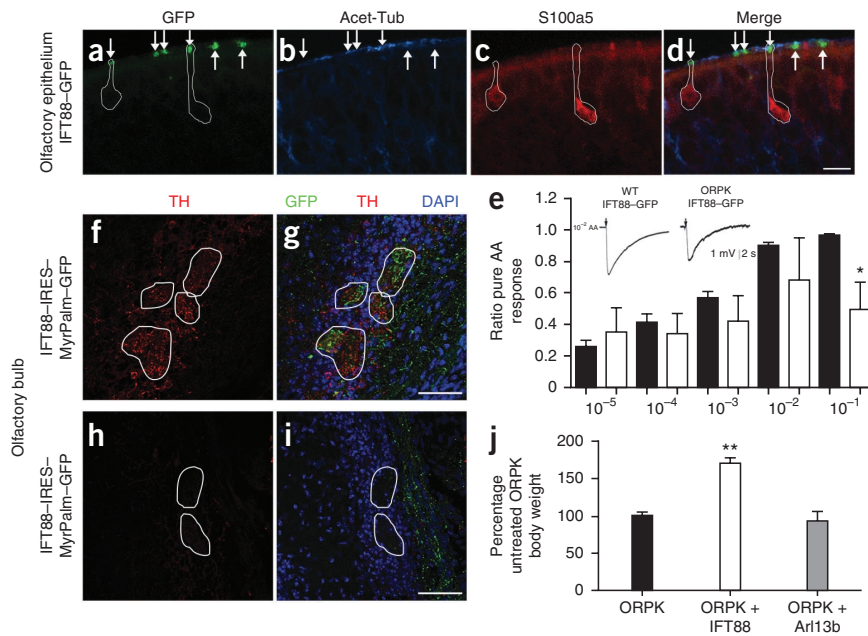


**Figure 3** Adenovirus-mediated expression of IFT88 in ORPK OSNs restores cilia and olfactory function. (a–d) Immunostaining for acetylated  $\alpha$ -tubulin (Acet-Tub) and S100a5 in the olfactory epithelium of ORPK mice infected with IFT88–GFP. Arrows mark GFP<sup>+</sup> OSN knobs. GFP<sup>+</sup> ORPK OSNs expressing S100a5 are circled. Scale bar, 10  $\mu$ m. (e) Quantified data of the EOG responses of WT (filled bars) and ORPK mice treated with IFT88–GFP (empty bars) to the indicated dilutions of amyl acetate (AA) (x axis).  $n = 5$  mice per group. \* $P < 0.05$  by Student's  $t$  test. Data are means  $\pm$  s.e.m. (f, g) Axons from ORPK OSNs expressing IFT88–IRES–MyrPalm–GFP innervating several glomeruli visualized by staining for GFP. Within and around these glomeruli, tyrosine hydroxylase (TH)<sup>+</sup> fibers and cells are present. (h, i) Immunostaining for tyrosine hydroxylase around glomeruli that lack axonal innervation from ORPK OSNs expressing IFT88–IRES–MyrPalm–GFP. Indicate for g and i. (j) Normalized body weights of untreated ORPK mice and ORPK mice treated with IFT88–GFP or Arl13b–mCherry. The body weights are normalized to the untreated ORPK mice.  $n = 3$  mice per group. \*\* $P < 0.005$  by one-way analysis of variance. Data are means  $\pm$  s.e.m.

the cilia labeled with Arl13b–mCherry (Supplementary Fig. 2m–o). Together, this indicates that ectopically expressed IFT88–GFP functions similarly to the endogenous protein and highlights its potential utility for restoring lost IFT88 activity.

To rescue the ORPK olfactory phenotype, we intranasally injected ORPK mice with IFT88–GFP adenovirus. When expressed in ORPK mice, IFT88–GFP restored acetylated  $\alpha$ -tubulin staining surrounding the dendritic knobs specifically in the infected OSNs (Fig. 3 and Supplementary Fig. 3). En face imaging of IFT88–GFP in ORPK OSNs showed a pattern of enrichment in the proximal regions of cilia identical to that present in WT OSNs (Supplementary Fig. 4). In addition to restoring cilia structures, intranasal delivery of IFT88–GFP also resulted in a mosaic pattern of expression of S100a5, presumably reflecting the extent of environmental-odor stimulation in each infected OSN (Fig. 3a–d). The intensity of S100a5 staining in the ORPK OSNs was comparable to the levels of expression observed in OSNs from WT mice. Individual ORPK OSNs infected with IFT88–GFP showed expression of S100a5, indicating that those neurons were active (Fig. 3a–d), whereas uninfected OSNs did not express S100a5. Adenoviral infection itself did not induce S100a5 expression, as we could detect activity-negative (S100a5-low) OSNs in infected WT olfactory epithelium (Supplementary Fig. 3i–p). Given that the effects of adenovirus-mediated expression of ectopic genes in OSNs can be measured by EOG responses to odorant stimulation<sup>32,33</sup>, we tested the hypothesis that restoration of cilia in individual ORPK OSNs was sufficient to restore the summated EOG response.

EOG recordings from ORPK mice infected with IFT88–GFP showed robust responses to increasing concentrations of amyl acetate, similar to the responses seen in WT littermates (Fig. 3e). Expression of IFT88–GFP in WT mice did not result in altered EOG responses compared to uninfected WT mice (Supplementary Fig. 5a). Together, these data show that expression of ectopic IFT88 rescues the EOG response in the olfactory epithelium and that this effect is specific to the restoration of cilia in the ORPK mouse.

We next tested whether the restored neuronal activity within the cell body was transmitted in the olfactory bulb. To trace the axons of infected OSNs to the olfactory bulb, we generated a bicistronic adenovirus construct that expressed both IFT88 and MyrPalm–GFP (Supplementary Fig. 3e–h). Using this bicistronic adenovirus construct, we traced axons from infected ORPK OSNs back to discrete glomeruli to determine whether expression of tyrosine hydroxylase was restored. Expression of IFT88–internal ribosomal entry site (IRES)–MyrPalm–GFP in ORPK OSN enhanced tyrosine hydroxylase staining in and around glomeruli that contained axons from infected OSNs (Fig. 3f, g and Supplementary Fig. 5b). Glomeruli within the same tissue section that did not contain GFP<sup>+</sup> axons did not show tyrosine hydroxylase expression (Fig. 3h, i). Thus expression of IFT88 in ORPK OSNs restores odorant-evoked activity that is transmitted

to the olfactory bulb. Adenoviral-mediated expression of Arl13b–mCherry in ORPK OSNs did not restore olfactory cilia structures and did not rescue olfactory function, showing the specificity of restored expression of IFT88 (Supplementary Fig. 6).

The lethality of the ORPK mutation precludes behavioral testing in adult mice. Suckling and feeding, however, are innate behaviors that are mediated by olfactory function<sup>34,35</sup> and are shared among all mammalian newborns<sup>36</sup>. Therefore, we tested whether the restored expression of IFT88 in OSNs was sufficient to subservise odor-guided feeding behavior<sup>36</sup>. By 3 weeks of age, surviving ORPK mice are approximately one-quarter the size of WT littermates<sup>37</sup>. ORPK mice infected with IFT88–GFP showed a ~60% increase in body weight compared to both untreated ORPK mice and ORPK mice infected with Arl13b–mCherry (Fig. 3j).

Given the continual presence of both mature and immature OSNs, we tested the specificity of adenoviral infection in the olfactory epithelium. Twenty-four hours after infection, more than 90% of infected neurons were mature, OMP<sup>+</sup> OSNs, and the expression of OMP persisted for a minimum of 1 month after infection (Supplementary Fig. 7a–j). To show that restored expression of IFT88 in mature OSNs can restore cilia structures, we used both fate mapping and adenoviral pulse chase to label mature ORPK OSNs before delivery of IFT88. We injected timed pregnant mice with BrdU at embryonic day 14.5 and analyzed them 14 d later (P7), when all the embryonically labeled BrdU<sup>+</sup> OSNs were fully mature, as determined by colabeling with OMP (Supplementary Fig. 7k–p). An analysis of ORPK mice

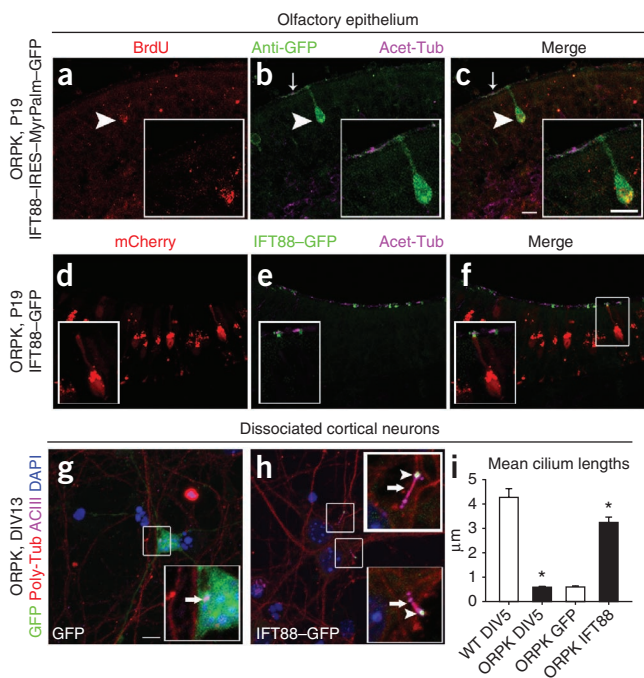


**Figure 4** Cilia are restored in mature neurons. (a–c) Immunostaining for acetylated  $\alpha$ -tubulin (Acet-Tub) around ORPK BrdU<sup>+</sup> OSNs infected with IFT88–IRES–MyrPalm–GFP. Anti-GFP, GFP-specific antibodies. (d–f) Immunostaining for acetylated  $\alpha$ -tubulin (Acet-Tub) around ORPK mCherry<sup>+</sup> OSNs infected with IFT88–GFP. (g,h) Immunostaining of day 13 *in vitro* (DIV13) ORPK neurons expressing GFP (g) or IFT88–GFP (h) for both polyglutamylated  $\alpha$ -tubulin (Poly-Tub) and ACIII. Arrows indicate cilia, and arrowheads highlight IFT88–GFP at the cilia tips (insets). (i) Quantification of cilia lengths of WT (4.3  $\mu$ m,  $n = 41$ ) and ORPK (0.6  $\mu$ m,  $n = 44$ ) neurons at DIV5 and cilia lengths of ORPK neurons infected with GFP (0.6  $\mu$ m,  $n = 20$ ) or IFT88–GFP (3.3  $\mu$ m,  $n = 20$ ) at DIV13. \* $P < 0.0001$  by Student's  $t$  test. Data are means  $\pm$  s.e.m. Scale bars, 10  $\mu$ m.

infected with IFT88–IRES–MyrPalm–GFP showed the restoration of cilia structures to infected BrdU<sup>+</sup> mature OSNs (Fig. 4a–c). In a second experiment, we first pulse labeled ORPK OSNs by infecting mice with an adenovirus construct encoding mCherry at ages P4 and P5. At 4 d after infection (P9) all mCherry-labeled OSNs were mature OMP<sup>+</sup> neurons (Supplementary Fig. 7q–v). Subsequent infection with IFT88–GFP (at P9 and P10) and an analysis performed 10 d later (at P19) showed that the first viral infusion of mCherry persisted and a population of these neurons was reinfected by the second infusion of IFT88–GFP. Immunostaining for acetylated  $\alpha$ -tubulin of dually labeled ORPK OSNs showed the restoration of cilia structures to mature OSNs (Fig. 4d–f). Then, to investigate whether restored expression of IFT88 can restore cilia to terminally differentiated neurons outside of the olfactory system, we dissociated cortical neurons from WT and ORPK mice. Cortical neurons from ORPK mice lacked discernable primary cilia compared to neurons from WT mice (Supplementary Fig. 8a–f). Adenoviral expression of IFT88–GFP in ORPK neurons restored cilia, as shown by both ACIII and polyglutamylated  $\alpha$ -tubulin staining (Fig. 4g–i).

Gene therapy has major potential for treating ciliopathies, especially because almost all mutations reported in patients, including those in the present work, are loss-of-function alleles. Our studies show the therapeutic rescue of a phenotype involving malformed cilia or loss of cilia on a differentiated cell. Treating the olfactory epithelium of ORPK mice with IFT88 adenovirus not only restored cilia to the

OSNs but also restored olfactory function at the cellular and behavioral level. Given that the olfactory epithelium undergoes constitutive neurogenesis throughout life, the duration of exogenously expressed proteins will probably be limited by the lifespan of the neurons, and, therefore, stable incorporation of adenovirally delivered genes in the OSNs may not be therapeutically necessary. However, the advantage of the olfactory system is its accessibility to noninvasive delivery methods. Future strategies for stable incorporation into the olfactory epithelial stem cell population may circumvent the necessity for repeated delivery and potential inflammatory side effects. Regardless, this work may provide a route for the palliation of some patients with a ciliopathy and provides a first proof of principle for gene therapy as a viable curative therapeutic approach to cilia disorders.

## METHODS

Methods and any associated references are available in the online version of the paper.

Note: Supplementary information is available in the online version of the paper.

## ACKNOWLEDGMENTS

This work was supported by US National Institutes of Health grants R01DC009606 (J.R.M.), F32DC011990 (J.C.M.), R01DC004553, R01DC008295 (R.R.R.), R01DK75996 (B.K.Y.), R01EY021872 (E.E.D.), R01HD04260, R01DK072301 and R01DK075972 (N.K.), by l'Agence National pour la Recherche (ANR) 2010 FOETOCILPATH 1122 01 (T.A.-B.) and by the University of Alabama at Birmingham Hepatorenal Fibrocystic Disease Core Center (DK074083). E.E.D., C.A.J., P.L.B. and N.K. are supported by the European Community's Seventh Framework Programme FP7/2009 under grant agreement 241955, SYSCILIA. N.K. is a Distinguished Jean and George W. Brumley Professor. We thank P. Loget for referring the family for this study, S. Dugan-Rocha, U. Nagaswamy and A. Hawes for assistance with mutational screening and R. Margolskee (Mount Sinai School of Medicine of New York University) for providing antibodies.

## AUTHOR CONTRIBUTIONS

J.C.M., E.E.D., A.J., I.-C.T., S.T., K.S., P.M.J., D.P.M., L.Z. and J.E. performed experiments. T.A.-B., P.L.B. and C.A.J. provided patients for mutational analysis. E.D.G., J.C.M., the NISC Comparative Sequencing Program, A.S., D.M.M. and R.A.G. performed the mutational analysis. J.C.M., P.M.J., D.P.M., E.E.D., N.K., R.R.R., C.L.W., B.K.Y. and J.R.M. designed experiments. All authors contributed insight towards shaping the aims of the project. J.C.M. and J.R.M. wrote the manuscript with the help of comments and suggestions from all other authors.

## COMPETING FINANCIAL INTERESTS

The authors declare no competing financial interests.

Published online at <http://www.nature.com/doi/10.1038/nm.2860>.

Reprints and permissions information is available online at <http://www.nature.com/reprints/index.html>.

- Rosenbaum, J.L. & Witman, G.B. Intraflagellar transport. *Nat. Rev. Mol. Cell Biol.* **3**, 813–825 (2002).
- Sharma, N., Berbari, N.F. & Yoder, B.K. Ciliary dysfunction in developmental abnormalities and diseases. *Curr. Top. Dev. Biol.* **85**, 371–427 (2008).
- Lancaster, M.A. & Gleason, J.G. The primary cilium as a cellular signaling center: lessons from disease. *Curr. Opin. Genet. Dev.* **19**, 220–229 (2009).
- Badano, J.L., Mitsuma, N., Beales, P.L. & Katsanis, N. The ciliopathies: an emerging class of human genetic disorders. *Annu. Rev. Genomics Hum. Genet.* **7**, 125–148 (2006).
- Lehman, J.M. *et al.* The Oak Ridge Polycystic Kidney mouse: modeling ciliopathies of mice and men. *Dev. Dyn.* **237**, 1960–1971 (2008).
- McEwen, D.P. *et al.* Hypomorphic CEP290/NPHP6 mutations result in anosmia caused by the selective loss of G proteins in cilia of olfactory sensory neurons. *Proc. Natl. Acad. Sci. USA* **104**, 15917–15922 (2007).
- Kulaga, H.M. *et al.* Loss of BBS proteins causes anosmia in humans and defects in olfactory cilia structure and function in the mouse. *Nat. Genet.* **36**, 994–998 (2004).
- Tadenev, A.L. *et al.* Loss of Bardet-Biedl syndrome protein-8 (BBS8) perturbs olfactory function, protein localization, and axon targeting. *Proc. Natl. Acad. Sci. USA* **108**, 10320–10325 (2011).
- Coon, B.G. *et al.* The Lowe syndrome protein OCL1 is involved in primary cilia assembly. *Hum. Mol. Genet.* **21**, 335–347 (2012).

10. Bretrup, C. *et al.* Ciliopathies with skeletal anomalies and renal insufficiency due to mutations in the IFT-A gene *WDR19*. *Am. J. Hum. Genet.* **89**, 634–643 (2011).
11. Valente, E.M. *et al.* Mutations in *TMEM216* perturb ciliogenesis and cause Joubert, Meckel and related syndromes. *Nat. Genet.* **42**, 619–625 (2010).
12. Merrill, A.E. *et al.* Ciliary abnormalities due to defects in the retrograde transport protein DYNC2H1 in short-rib polydactyly syndrome. *Am. J. Hum. Genet.* **84**, 542–549 (2009).
13. Walczak-Sztulpa, J. *et al.* Cranioectodermal Dysplasia, Sensenbrenner syndrome, is a ciliopathy caused by mutations in the IFT122 gene. *Am. J. Hum. Genet.* **86**, 949–956 (2010).
14. Kozminski, K.G., Johnson, K.A., Forscher, P. & Rosenbaum, J.L. A motility in the eukaryotic flagellum unrelated to flagellar beating. *Proc. Natl. Acad. Sci. USA* **90**, 5519–5523 (1993).
15. Kozminski, K.G., Beech, P.L. & Rosenbaum, J.L. The Chlamydomonas kinesin-like protein FLA10 is involved in motility associated with the flagellar membrane. *J. Cell Biol.* **131**, 1517–1527 (1995).
16. Arts, H.H. *et al.* *C14ORF179* encoding IFT43 is mutated in Sensenbrenner syndrome. *J. Med. Genet.* **48**, 390–395 (2011).
17. Beales, P.L. *et al.* *IFT80*, which encodes a conserved intraflagellar transport protein, is mutated in Jeune asphyxiating thoracic dystrophy. *Nat. Genet.* **39**, 727–729 (2007).
18. Davis, E.E. *et al.* *TTC21B* contributes both causal and modifying alleles across the ciliopathy spectrum. *Nat. Genet.* **43**, 189–196 (2011).
19. Gilissen, C. *et al.* Exome sequencing identifies *WDR35* variants involved in Sensenbrenner syndrome. *Am. J. Hum. Genet.* **87**, 418–423 (2010).
20. Friedland-Little, J.M. *et al.* A novel murine allele of Intraflagellar Transport Protein 172 causes a syndrome including VACTERL-like features with hydrocephalus. *Hum. Mol. Genet.* **20**, 3725–3737 (2011).
21. Pazour, G.J. *et al.* Chlamydomonas *IFT88* and its mouse homologue, polycystic kidney disease gene *tg737*, are required for assembly of cilia and flagella. *J. Cell Biol.* **151**, 709–718 (2000).
22. Willaredt, M.A. *et al.* A crucial role for primary cilia in cortical morphogenesis. *J. Neurosci.* **28**, 12887–12900 (2008).
23. Liu, A., Wang, B. & Niswander, L.A. Mouse intraflagellar transport proteins regulate both the activator and repressor functions of Gli transcription factors. *Development* **132**, 3103–3111 (2005).
24. Leitch, C.C. *et al.* Hypomorphic mutations in syndromic encephalocele genes are associated with Bardet-Biedl syndrome. *Nat. Genet.* **40**, 443–448 (2008).
25. Zaghoul, N.A. *et al.* Functional analyses of variants reveal a significant role for dominant negative and common alleles in oligogenic Bardet-Biedl syndrome. *Proc. Natl. Acad. Sci. USA* **107**, 10602–10607 (2010).
26. Khanna, H. *et al.* A common allele in *RPGRIP1L* is a modifier of retinal degeneration in ciliopathies. *Nat. Genet.* **41**, 739–745 (2009).
27. Acland, G.M. *et al.* Gene therapy restores vision in a canine model of childhood blindness. *Nat. Genet.* **28**, 92–95 (2001).
28. Pawlyk, B.S. *et al.* Gene replacement therapy rescues photoreceptor degeneration in a murine model of Leber congenital amaurosis lacking RPGRIP. *Invest. Ophthalmol. Vis. Sci.* **46**, 3039–3045 (2005).
29. Simons, D.L., Boye, S.L., Hauswirth, W.W. & Wu, S.M. Gene therapy prevents photoreceptor death and preserves retinal function in a Bardet-Biedl syndrome mouse model. *Proc. Natl. Acad. Sci. USA* **108**, 6276–6281 (2011).
30. Bennett, M.K., Kulaga, H.M. & Reed, R.R. Odor-evoked gene regulation and visualization in olfactory receptor neurons. *Mol. Cell. Neurosci.* **43**, 353–362 (2010).
31. Baker, H., Kawano, T., Margolis, F.L. & Joh, T.H. Transneuronal regulation of tyrosine hydroxylase expression in olfactory bulb of mouse and rat. *J. Neurosci.* **3**, 69–78 (1983).
32. Zhao, H. *et al.* Functional expression of a mammalian odorant receptor. *Science* **279**, 237–242 (1998).
33. Ivic, L. *et al.* Adenoviral vector-mediated rescue of the OMP-null phenotype *in vivo*. *Nat. Neurosci.* **3**, 1113–1120 (2000).
34. Risser, J.M. & Slotnick, B.M. Nipple attachment and survival in neonatal olfactory bulbectomized rats. *Physiol. Behav.* **40**, 545–549 (1987).
35. Brunet, L.J., Gold, G.H. & Ngai, J. General anosmia caused by a targeted disruption of the mouse olfactory cyclic nucleotide-gated cation channel. *Neuron* **17**, 681–693 (1996).
36. Varendi, H., Porter, R.H. & Winberg, J. Does the newborn baby find the nipple by smell? *Lancet* **344**, 989–990 (1994).
37. Sommardahl, C.S., Woychik, R.P., Sweeney, W.E., Avner, E.D. & Wilkinson, J.E. Efficacy of taxol in the orpk mouse model of polycystic kidney disease. *Pediatr. Nephrol.* **11**, 728–733 (1997).

## ONLINE METHODS

**Ciliopathy mutational screening.** Genomic DNA was obtained from fetuses with JATD, MKS or MKS-like features (prenatal- or neonatal-lethal samples with overlapping MKS features but not all of the clinical diagnostic MKS criteria) or their family members after informed consent. We amplified the exon sequence and intron-exon junctions of *IFT88* from the DNA according to standard protocols<sup>18</sup>; variants were confirmed by resequencing and visual assessment of chromatograms. Primer sequences and PCR conditions are available on request. These studies were approved by the Institutional Review Board or equivalent ethics boards at Duke University, Necker Hospital, St. James's University Hospital and University College London.

**Zebrafish embryo injections.** *ift88* MO<sup>38,39</sup> (Gene Tools) was injected into WT zebrafish embryos at the 1–4 cell stage<sup>18</sup>. We inserted a full-length IFT88 human open reading frame in the pCS2+ vector and transcribed mRNA from linearized WT and mutant constructs with the SP6 mMessage mMachine kit (Ambion). Injection cocktails contained MO, mRNA or combinations of MO and mRNA (3 ng MO and 100 pg mRNA in each instance). We conducted live phenotypic scoring at the 9–10 somite stage, as previously defined<sup>18</sup>. Live embryo images were captured at 8× magnification on a Nikon AZ100 using a Nikon digital sight camera and NIS Elements software.

**mIMCD3 transfections.** We generated cell lines of mIMCD3 cells stably expressing shRNA targeting mouse *Ift88* (TRCN0000181620, Sigma) or control shRNA targeting no known mammalian gene (SHC002, Sigma). After selection with puromycin (5 µg/ml; Sigma) cells were transfected using Fugene HD (Roche) with 1 µg DNA per well (pCAG-V5-EV-IRES-enhanced GFP (eGFP)-pA or pCAG-V5-IFT88 (WT or M383K)-IRES-eGFP-pA). pHRGFP-IIN plasmid (Stratagene; 100 ng/well) was co-transfected as a control. After serum starvation cells were fixed with 100% methanol for immunofluorescent staining, as previously described<sup>18</sup>. Twelve to fourteen different fields were chosen randomly for imaging at 60× magnification with a Nikon 90i fluorescent microscope to determine the percentage of ciliated cells. Pairwise comparisons to WT for rescue efficiency were conducted using a  $\chi^2$  test.

**Adenovirus preparation.** IFT88-GFP, IFT88-IRES-MyrPalm-GFP, Arl13b-mCherry, GFP and mCherry were inserted into the adenoviral vector pAD/V5-dest, and the virus was produced following the ViraPower protocol (Invitrogen). The amplified virus was purified with the Virapur Adenovirus mini purification Virakit (Virapur, San Diego, CA), which was followed by dialyzed into a solution of 2.5% glycerol, 25 mM NaCl and 20 mM Tris-HCl, pH 8.0, at 4 °C overnight before storing it at –80 °C.

**Mice and infections.** ORPK mice on a FVB/N background (provided by B.K.Y.) were bred and maintained at the University of Michigan. All procedures were approved by the University Committee for the Use and Care of Animals. EOG recordings were performed on the mice between the ages of P16 and P21. Pups were intranasally infected with 20 µl of adenovirus constructs at P7, and infection was repeated for 3 consecutive days.

**EOGs.** EOGs were recorded as previously described<sup>6</sup>. Briefly, electrodes ranging from 1–4 MΩ in resistance were placed on either turbinate II or IIb for recordings. Data was analyzed with Clampfit (Molecular Devices, Sunnyvale, CA) to determine the peak heights from the prepulse baseline. At least three mice were tested for each condition.

**Primary neuron culture.** Dissociated P1 mouse cortical neurons were plated at 50,000 cells per dish in poly-D-lysine-coated glass-bottom 35-mm Petri dishes (MatTek). Cells were maintained at 37 °C in growth medium (Neurobasal A supplemented with B27 and Glutamax-1 (Invitrogen)). DIV6 neurons were infected with either GFP or IFT88-GFP adenovirus in Neurobasal A medium for 2 h. After 2 h, the media was replaced with growth medium, and cells were maintained until DIV13. Measurements of the cilia lengths of the dissociated cortical neurons were made from confocal images of ACIII staining using ImageJ software.

**Olfactory epithelium immunofluorescence.** After transcardial perfusion with 4% paraformaldehyde (PFA), dissected heads from the mice were incubated in 4% PFA for 2–12 h and decalcified in 0.5 M EDTA and 1× PBS overnight at 4 °C. Snouts were then cryoprotected in 10%, 20% and 30% sucrose for 1 h, 1 h and overnight, respectively, at 4 °C, frozen in optimal cutting temperature (OCT) compound (Sakura Finetek, Torrance, CA) and cut into sections (10–12 µm) on a cryostat. Immunofluorescence staining on olfactory tissue was performed as previously described<sup>6</sup>.

The antibodies used were as follows: monoclonal antibody to acetylated  $\alpha$ -tubulin (1:1,000, T6793 Sigma-Aldrich, St. Louis, MO), polyclonal antibody to ACIII (1:500, SC588, Santa Cruz Biotechnology, Santa Cruz, CA), polyclonal antibody to  $\gamma$ 13 (1:500, R. Margolskee, Mount Sinai School of Medicine of New York University, New York, NY), polyclonal antibody to IFT88 (1:500, B.K.Y.), polyclonal antibody to S100a5 (1:200, R.R.R.), polyclonal antibody to tyrosine hydroxylase (1:500, MAB318, Millipore), polyclonal antibody to OMP (1:1,000, 544-10001, Wako), polyclonal antibody to growth-associated protein 43 (Gap43) (1:500, AB9854, Millipore), polyclonal antibody to CNGA2 (1:250, APC-045, Alomone Labs, Jerusalem, Israel), polyclonal antibody to GFP (rabbit; 1:1,000, A-6455, Molecular Probes; chicken; 1:500, A01694, Gen Script USA), monoclonal antibody to polyglutamylated  $\alpha$ -tubulin (1:1,000, ALX-804-885-C100, Enzo Life Sciences) and Alexa-Fluor conjugated secondary antibodies (1:1,000, Invitrogen, Carlsbad, CA).

**En face imaging.** Mice were euthanized with CO<sub>2</sub> and decapitated, and their olfactory turbinates were removed, placed against a glass cover slip and held in place with a tissue slice holder (Warner Instruments). Images were collected on an Olympus Fluoview 500 confocal microscope with a 60× 1.4 numerical aperture oil objective.

**Scanning electron microscopy.** Mice were transcardially perfused with 2% glutaraldehyde, 0.15 M cacodylate in water and post-fixed at 4 °C overnight. The olfactory epithelium was prepared for scanning electron microscopy using a variation of the OTOTO method<sup>40</sup>, critical point dried and mounted on stubs. The samples were examined with an Amray (Drogheda, Ireland) 1910FE field emission scanning electron microscope at 5 kV and recorded digitally with Semicaps software.

38. Bisgrove, B.W., Snarr, B.S., Emrazian, A. & Yost, H.J. Polaris and Polycystin-2 in dorsal forerunner cells and Kupffer's vesicle are required for specification of the zebrafish left-right axis. *Dev. Biol.* **287**, 274–288 (2005).

39. Tsujikawa, M. & Malicki, J. Intraflagellar transport genes are essential for differentiation and survival of vertebrate sensory neurons. *Neuron* **42**, 703–716 (2004).

40. Malick, L.E. & Wilson, R.B. Modified thiocarbonylhydrazide procedure for scanning electron microscopy: routine use for normal, pathological, or experimental tissues. *Stain Technol.* **50**, 265–269 (1975).